

Two-Pion Exchange Contributions to the Nucleon-Nucleon Interaction from the Roper Resonance

Yang Xiao,^{1, 2, 3} Li-Sheng Geng,^{3, 4, 5, 6,*} and U. van Kolck^{7, 8, 9, †}

¹*Center for Exotic Nuclear Studies, Institute for Basic Science, Daejeon 34126, Republic of Korea*

²*School of Space and Environment, Beihang University, Beijing 102206, China*

³*School of Physics, Beihang University, Beijing 102206, China*

⁴*Sino-French Carbon Neutrality Research Center,*

École Centrale de Pékin/School of General Engineering,

Beihang University, Beijing 100191, China

⁵*Peng Huanwu Collaborative Center for Research and Education,*

Beihang University, Beijing 100191, China

⁶*Southern Center for Nuclear-Science Theory (SCNT),*

Institute of Modern Physics, Chinese Academy of Sciences, Huizhou 516000, China

⁷*European Centre for Theoretical Studies in Nuclear Physics and Related Areas (ECT*),*

Fondazione Bruno Kessler, 38123 Villazzano (TN), Italy

⁸*Université Paris-Saclay, CNRS/IN2P3, IJCLab, 91405 Orsay, France*

⁹*Department of Physics, University of Arizona, Tucson, AZ 85721, USA*

We derive the long-range components of the nucleon-nucleon (NN) two-pion-exchange potential with an intermediate Roper resonance. Leading-order interactions in heavy-baryon chiral perturbation theory are considered. NN phase shifts with orbital angular momentum $L \geq 2$ are calculated in first-order perturbation theory and compared to those obtained without the Roper resonance. We show that the Roper contribution is sizeable for D waves and improves the description of phase shifts for all the partial waves slightly. We also discuss the role of the Roper resonance in the NN interaction in the framework of resonance saturation.

I. INTRODUCTION

Nuclear interactions are a fundamental input in nuclear physics and astrophysics, which have been comprehensively studied in effective field theories (EFTs) of QCD since the early 1990s [1–7]. See Ref. [8] for a recent review. In Chiral EFT (χ EFT), nuclear forces have two types. The

*Email: lisheng.geng@buaa.edu.cn

†Email: vankolck@ijclab.in2p3.fr

lightness of the pion, guaranteed by spontaneous chiral-symmetry breaking and small quark masses, makes it responsible for long-range interactions through one or more exchanges. The short-range interactions encode details of QCD dynamics at distances $r \lesssim M_{\text{QCD}}^{-1}$, where $M_{\text{QCD}} \sim 1$ GeV is the characteristic nonperturbative scale of the theory associated with most baryon masses, such as the nucleon's $m_N \simeq 940$ MeV. While determining the low-energy constants (LECs) associated with contact interactions requires nuclear input, the long-range potential can be calculated using LECs obtained from one-baryon processes. Here, we examine a novel long-range component of the nucleon-nucleon (NN) interaction.

Long-range NN forces are expected to be amenable to the power counting employed in χ EFT restricted to at most one nucleon, chiral perturbation theory [9]. The leading-order (LO) long-range potential comes from the well-known static one-pion exchange (OPE), with two-pion exchange (TPE) as the first correction. Since the first derivations [5, 7, 10, 11], much work has been devoted to calculations of these forces in an explicit nonrelativistic expansion based on heavy-baryon chiral perturbation theory (HB χ PT) [12, 13]. Together with a prescription for the ordering of short-range interactions, OPE and TPE have led to many phenomenologically successful chiral potentials as reviewed in, for example, Refs. [8, 14, 15]. In recent years, a relativistically covariant EFT has been proposed and found to converge faster than these conventional chiral potentials [16–28].

Most existing chiral nuclear forces contain only the ground-state nucleon, with the contributions from baryon excited states relegated to LECs at higher orders. State-of-the-art chiral nuclear forces have been constructed up to the fifth order in the nonrelativistic formalism [29] and up to the third order in the covariant formalism [24]. Although already of high precision, these chiral nuclear forces still encounter some problems, *e.g.*, convergence with respect to the components of the TPE potential. It has long been realized [5, 7, 10] that the formally subleading component of TPE is comparable or even larger than the presumably leading TPE, which challenges the power counting underlying χ EFT. It has even been proposed [30–33] that TPE should be promoted to LO together, or even replace OPE.

The convergence issues of chiral nuclear forces can be ameliorated by explicitly including baryon resonances. If the effects of a resonance are relegated to LECs, non-analytic contributions are lost, which limits the expansion range of the theory. Including a low-lying resonance explicitly as a low-energy degree of freedom not only extends the validity of the EFT but also reorganizes the multipion-exchange contributions and improves order-by-order convergence. The lowest nucleon excitation is the Delta isobar, $\Delta(1232)$, whose mass m_Δ is only $\delta \equiv m_\Delta - m_N \simeq 300$ MeV higher than the nucleon's. Its contribution to NN [5, 7, 11, 34–39] and three-nucleon [6, 40–43]

chiral forces has attracted increasing attention. Delta effects, which would otherwise appear only in the subleading TPE via LECs, have already become manifest in the leading TPE. Moreover, some of the nuclear matter properties are also found to be better described in Deltaful chiral potentials [36, 37, 39, 44].

In TPE, a nucleon scatters a virtual pion. χ EFT can be extended to the Delta region in pion-nucleon scattering [45] following a similar approach to other hadronic reactions [46]. However, the P_{11} channel still converges poorly, unless the second nucleon excitation — the Roper resonance $N(1440)$ [47], lying $\rho \equiv m_R - m_N \simeq 500$ MeV above the nucleon — is introduced explicitly [48]. Unlike higher resonances, the Roper width is compatible with having an origin in the chiral expansion. The Roper also nearly saturates the Adler-Weisberger sum rule together with nucleon and Delta, which suggests that these baryons fall into a simple reducible representation of the chiral group [49, 50]. By now, several properties of the Roper have been studied in χ EFT [51–56].

The role of the Roper in chiral nuclear forces is explored here for the first time. Previous calculations of Roper effects in the NN system predate χ EFT. They were based on coupled-channel approaches, with an emphasis on the pion-production region and above; see, for example, Refs. [57–60]. Here, we derive the TPE NN potential with one and two intermediate Ropers in HB χ PT. This potential is to be employed in conjunction with other components of the chiral nuclear force, with an eye to future extensions into the pion-production region. Our main focus here is the Roper, not the much more studied Delta isobar. As we are going to see, the Roper contributions are relatively small at low energies, and in this first approach, we disregard combined Delta and Roper contributions. We compare the Roper TPE to the formerly leading TPE containing only nucleons in intermediate states and calculate its effects on the NN elastic scattering phase shifts for partial waves with orbital angular momentum $L \geq 2$, where the centrifugal barrier favors the use of perturbation theory. The contribution from intermediate Roper resonances is found to be sizeable for D waves and yields a slightly better description of the phase shifts across all partial waves. We also discuss the role of the Roper resonance from the perspective of resonance saturation.

The manuscript is organized as follows. In Sec. II, we provide the effective Lagrangian relevant to our study and calculate the leading TPE potential with one and two intermediate Roper resonances. The isoscalar and isovector TPE potentials in momentum space and the resulting NN scattering phase shifts for $L \geq 2$ are shown and discussed in Sec. III. A summary and outlook are given in Sec. IV.

II. ROPER CONTRIBUTIONS TO NUCLEON-NUCLEON SCATTERING

In this section, we derive the long-range components of the leading TPE potential in the presence of intermediate Roper resonances. After the relevant terms in the Lagrangian are presented in Sec. II A, the various diagrams — triangle and (planar and crossed) box — with one and two Ropers are examined in Sec. II B.

A. Effective Lagrangian

The Roper has the same quantum numbers (spin $S = 1/2$ and isospin $I = 1/2$) as the nucleon and therefore both can be represented by isospinor spinor fields, which we denote as R and N , respectively. Since we are interested in the nonrelativistic regime where antibaryons only contribute to short-range effects, we can use heavy particle fields [12, 13], each with two components representing particle spin states. The inert nucleon mass is removed through a phase redefinition, leaving behind the Roper-nucleon mass difference $\rho \equiv m_R - m_N$. The baryon covariant velocity is denoted by v_μ and covariant spin operator is $S_\mu = i\gamma_5\sigma_{\mu\nu}v^\nu/2$. We will work in the baryons' rest frame, where $v_\mu = (1, 0, 0, 0)$ and $S_\mu = (0, \vec{\sigma}/2)$ in terms of the Pauli spin matrices $\vec{\sigma}$. The contributions from antibaryons are represented in the EFT by contact interactions.

In addition, we focus on momenta comparable to the pion mass, where the isospin-triplet π of pseudoscalar pions needs to be considered explicitly. Pions are pseudo-Goldstone bosons of spontaneous chiral $SU(2) \times SU(2)$ symmetry breaking, characterized by the pion decay constant $f_\pi \simeq 92$ MeV. Chiral symmetry is realized nonlinearly [61], for example through the use of a field [62, 63] $U(x) = u^2(x) = \exp(i\boldsymbol{\pi} \cdot \boldsymbol{\tau}/f_\pi)$, where $\boldsymbol{\tau}$ are the Pauli matrices in isospin space. Chiral symmetry is implemented easily through chiral-covariant derivatives

$$u_\mu = i \left(u^\dagger \partial_\mu u - u \partial_\mu u^\dagger \right), \quad (1)$$

$$D_\mu \Psi = \partial_\mu \Psi + \frac{1}{2} [u^\dagger \partial_\mu u + u \partial_\mu u^\dagger, \Psi], \quad (2)$$

for the pion field and a spin-1/2 field Ψ , respectively.

To calculate the leading TPE potential with the Roper resonance in $\text{HB}\chi\text{PT}$, we need the

leading terms in the effective chiral Lagrangian including pions, nucleon, and Roper [48],

$$\begin{aligned}\mathcal{L}^{(0)} = & \frac{f_\pi^2}{4} \text{Tr} \left[(\partial_\mu U)(\partial^\mu U^\dagger) + m_\pi^2 (U + U^\dagger) \right] + \bar{N} (iv \cdot D + g_A S \cdot u) N \\ & + \bar{R} (iv \cdot D - \rho) R + g'_A (\bar{R} S \cdot u N + \text{H.c.}) ,\end{aligned}\quad (3)$$

where g_A and g'_A are the axial-vector coupling of the pion to the nucleon and the transition nucleon-Roper coupling, respectively. Subleading terms include more derivatives, powers of the pion mass, and powers of the Roper-nucleon mass difference. Among the higher-order terms, one also finds isospin-breaking terms proportional to the quark-mass difference and the electromagnetic fine-structure constant. With naive dimensional analysis [64], which incorporates naturalness in a perturbative context [65], higher-order terms are suppressed by powers of $M_{\text{QCD}} \sim \Lambda_\chi \equiv 4\pi f_\pi$.

B. Two-pion exchange potential with intermediate Ropers

The nucleon propagator from the Lagrangian (3) is static. Two-nucleon reducible diagrams — that is, those that can be split by cutting only intermediate nucleon lines — have a pinch singularity and are infrared divergent, which requires [2] a resummation in the nucleon propagator of the recoil term proportional to m_N^{-1} appearing in the Lagrangian with an additional derivative, $\mathcal{L}^{(1)}$. These diagrams are then infrared finite but enhanced [8] by a factor of $4\pi m_N/p$, where p is the characteristic momentum of the process. The NN potential is defined as the sum of two-nucleon irreducible diagrams. Being free of the infrared divergence, contributions to the long-range potential can be estimated [2] with the same power counting of χ PT [9]. Neglecting isospin-breaking corrections, the long-range potential is a perturbative expansion in Q/M_{QCD} , where Q represents the low-energy scales: p , m_π , δ , and in our case ρ as well.

The leading contributions to the long-range NN potential from intermediate Roper resonances and nucleons arise from the Feynman diagrams shown in Fig. 1. These are all the one-loop diagrams one can build with the propagators and vertices extracted from the leading Lagrangian in Eq. (3) involving nucleons, Ropers, and pions. They represent contributions in Roperful χ EFT of $\mathcal{O}(Q^2/M_{\text{QCD}}^2)$ relative to OPE. Since there are no pinch singularities, baryons are static with recoil corrections expected at the next order. The Roper decay width, arising from the one-loop correction to the Roper propagator, enters two orders down in the chiral expansion. The triangle diagrams arise from the Weinberg-Tomozawa vertex contained in the nucleon chiral-covariant derivative and are proportional to g'_A^2 . The planar- and crossed-box diagrams are proportional to $g_A^2 g'_A^2$ or g'_A^4 ,

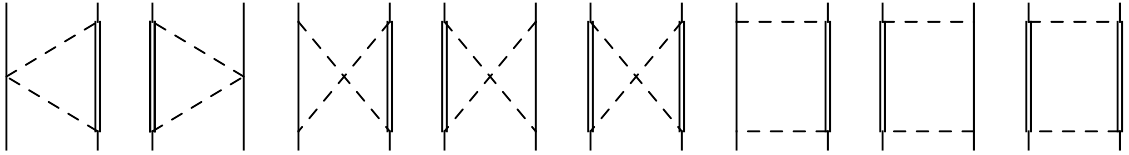


FIG. 1: Leading two-pion-exchange contributions to the two-nucleon potential with an intermediate Roper resonance. Solid, double, and dashed lines represent nucleons, Ropers, and pions, respectively. Propagators and vertices are from the Lagrangian $\mathcal{L}^{(0)}$, Eq. (3).

depending on whether they contain one or two intermediate Ropers. Note that there is always at least one resonance in intermediate states, and no subtraction of iterated OPE is needed.

Including the Roper also implies that one must consider explicit contributions from the Delta isobar, since the Delta isobar's mass is smaller than the Roper's. At the order we consider here, there are also box diagrams involving one Roper and one Delta in intermediate states, which are proportional to $h_A^2 g_A'^2$, where h_A is the axial-vector nucleon-Delta coupling analog to g_A' . These diagrams are independent of the diagrams considered here, and their evaluation is left for a subsequent publication.

As with any other loop diagrams, those in Fig. 1 require regularization. They contain short-range components that do not vanish when the regulator is removed. This regulator dependence can be eliminated by appropriately regulating the bare strengths of two-nucleon contact interactions. The asymptotic form of the potential is obtained at distances much larger than the inverse of the momentum cutoff; see, for example, Refs. [7, 66] for nucleon and Delta intermediate states. However, the same result is most cleanly obtained with dimensional regularization and minimal subtraction, which we employ in the following. The calculation is analogous to that in Refs. [10, 11].

We consider the diagrams in Fig. 1 in the center-of-mass (CM) frame and denote the initial and final momenta by \vec{p} and \vec{p}' , respectively, with $\vec{q} = \vec{p} - \vec{p}'$ the transferred momentum. Representing the spin and isospin operators of nucleon i by $\vec{\sigma}_i$ and τ_i , the corresponding potential takes the form

$$V = V_C + W_C \tau_1 \cdot \tau_2 + (V_S + W_S \tau_1 \cdot \tau_2) \vec{\sigma}_1 \cdot \vec{\sigma}_2 + (V_T + W_T \tau_1 \cdot \tau_2) \vec{\sigma}_1 \cdot \hat{q} \vec{\sigma}_2 \cdot \hat{q}, \quad (4)$$

where the subscripts C , S , and T refer to the central, spin-spin, and quasi-tensor components, respectively, with V denoting the isoscalar potential and W the isovector potential. (Note that, similar to Refs. [10, 11], we use an unconventional form for the tensor term, from which a spin-spin term $\vec{\sigma}_1 \cdot \vec{\sigma}_2/3$ is not subtracted.)

As can be expected in general, there are several cancellations among terms in planar and crossed boxes since only the sum of all diagrams with a given dependence on parameters like g_A and g_A' is

invariant under field redefinitions. Adding all diagrams, we obtain

$$V_C^{(1R)} = -\frac{3g_A'^2 g_A^2}{64\pi f_\pi^4 \rho} \left[m_\pi \omega^2(q) + (2m_\pi^2 + q^2)^2 A(q) \right], \quad (5)$$

$$V_C^{(2R)} = \frac{3g_A'^4}{128\pi^2 f_\pi^4} \left\{ -\omega^2(q) - \rho^2 - \frac{m_\pi^2 [4\rho^2 + \omega^2(q)] - 8\rho^4}{h\rho} \cosh^{-1} \frac{\rho}{m_\pi} \right. \\ \left. + 10\rho^2 \ln \frac{m_\pi}{\mu} + 2\rho^2 L(q) - (q^2 - 2h^2) \left(\frac{2m_\pi^2 + q^2}{4\rho^2} + \frac{3}{2} \right) f_1(q) + \frac{(q^2 - 2h^2)^2}{4\rho^2} f_2(q) \right\}, \quad (6)$$

for the isoscalar central component,

$$W_C^{(1R)} = \frac{g_A'^2 g_A^2}{32\pi^2 f_\pi^4} \left\{ 5m_\pi^2 + \frac{3}{2}q^2 - 2\rho^2 + 2 \left\{ \frac{m_\pi^2}{h\rho} \omega^2(q) - \frac{\rho}{h} [\omega^2(q) - 2h^2] \right\} \cosh^{-1} \frac{\rho}{m_\pi} \right. \\ \left. - [3\omega^2(q) - 4\rho^2] \ln \frac{m_\pi}{\mu} - (2m_\pi^2 + q^2) L(q) + (2m_\pi^2 + q^2) \frac{(q^2 - 2h^2)}{2\rho^2} f_1(q) \right\}, \quad (7)$$

$$W_C^{(2R)} = \frac{g_A'^4}{64\pi^2 f_\pi^4} \left\{ \frac{4}{3}m_\pi^2 + \frac{31}{36}q^2 - 6\rho^2 + \left\{ \frac{m_\pi^2}{h\rho} \omega^2(q) + \frac{\rho}{h} [12h^2 + 4\rho^2 - 2\omega^2(q)] \right\} \cosh^{-1} \frac{\rho}{m_\pi} \right. \\ \left. - \left(15m_\pi^2 + \frac{23}{6}q^2 - 20\rho^2 \right) \ln \frac{m_\pi}{\mu} - \left(\frac{10}{3}m_\pi^2 + \frac{11}{6}q^2 - 4\rho^2 \right) L(q) \right. \\ \left. + (2m_\pi^2 + q^2 - 10\rho^2) \frac{(q^2 - 2h^2)}{4\rho^2} f_1(q) + \frac{(q^2 - 2h^2)^2}{4\rho^2} f_2(q) \right\}, \quad (8)$$

for the isovector central component,

$$V_T^{(1R)} = -V_S^{(1R)} \quad (9)$$

$$= \frac{3g_A'^2 g_A^2 q^2}{64\pi^2 f_\pi^4} \left\{ 2 - \frac{h}{\rho} \cosh^{-1} \frac{\rho}{m_\pi} - 2 \ln \frac{m_\pi}{\mu} - L(q) + \left[\frac{\omega^2(q)}{4\rho^2} - 1 \right] f_1(q) \right\}, \quad (10)$$

$$V_T^{(2R)} = -V_S^{(2R)} \quad (11)$$

$$\begin{aligned} &= \frac{3g_A'^4 q^2}{256\pi^2 f_\pi^4} \left\{ 3 + \frac{m_\pi^2 - 2\rho^2}{h\rho} \cosh^{-1} \frac{\rho}{m_\pi} - 4 \ln \frac{m_\pi}{\mu} - 2L(q) \right. \\ &\quad \left. + \left(\frac{\omega^2(q)}{4\rho^2} - 3 \right) f_1(q) + \left(\frac{\omega^2(q)}{4\rho^2} - 1 \right) f_2(q) \right\}, \end{aligned} \quad (12)$$

for the isoscalar quasi-tensor and spin-spin components, and

$$W_T^{(1R)} = -W_S^{(1R)} \quad (13)$$

$$= -\frac{g_A'^2 g_A^2 q^2}{64\pi f_\pi^4 \rho} [m_\pi + \omega^2(q) A(q)], \quad (14)$$

$$W_T^{(2R)} = -W_S^{(2R)} \quad (15)$$

$$= -\frac{g_A'^4 q^2}{128\pi^2 f_\pi^4} \left[1 + \frac{m_\pi^2}{h\rho} \cosh^{-1} \frac{\rho}{m_\pi} + \left(\frac{\omega^2(q)}{4\rho^2} + 1 \right) f_1(q) - \left(\frac{\omega^2(q)}{4\rho^2} - 1 \right) f_2(q) \right], \quad (16)$$

for the isovector quasi-tensor and spin-spin components.

In the above equations, μ is the renormalization scale and the quantities h , ω , L , A , f_1 , and f_2 are defined as

$$h = \sqrt{\rho^2 - m_\pi^2}, \quad (17)$$

$$\omega(q) = \sqrt{4m_\pi^2 + q^2} \quad (18)$$

$$L(q) = \frac{\omega(q)}{2q} \ln \frac{(\omega(q) + q)^2}{4m_\pi^2} \quad (19)$$

$$A(q) = \frac{1}{2q} \tan^{-1} \frac{q}{2m_\pi} \quad (20)$$

$$f_1(q) = \int_0^1 dx F(q; x) \cot^{-1} F(q; x), \quad (21)$$

$$f_2(q) = \int_0^1 dx F^3(q; x) \cot^{-1} F(q; x) + \frac{4\rho^2}{q\sqrt{4h^2 - q^2}} \tan^{-1} \frac{q}{\sqrt{4h^2 - q^2}}, \quad (22)$$

$$F(q; x) = \left[\frac{q^2}{\rho^2} x(1-x) - \frac{h^2}{\rho^2} \right]^{-1/2}. \quad (23)$$

It is necessary to check the consistency between the TPE potentials with and without explicit Roper contributions. For this purpose, we set the Roper-nucleon mass splitting $\rho = 0$ and compare

the resulting potential to that in Ref. [10]. We find that they are identical.

This potential is local because it depends on momenta only through the momentum transfer \vec{q} . It contains analytic terms that cannot be separated from LECs. The necessity of LECs is evident from their explicit dependence on the renormalization scale μ . Had we used a momentum cutoff Λ , it would appear instead of μ and make it evident that the separation is arbitrary between TPE and short-range interactions at the same order. There are two (seven) independent contact interactions we can construct with no (two) powers of momenta [3, 7]. Accounting for explicit chiral-symmetry breaking, two more contact interactions appear with two powers of the pion mass. These LECs can remove all the analytic terms in Eqs. (5)–(16).

More interesting are the non-analytic terms in $q = |\vec{q}|$ that cannot be reproduced by a finite series of short-range interactions. They are independent of the regulator: they can be obtained instead for a momentum cutoff when $\Lambda \rightarrow \infty$. These non-analytic contributions display the expected suppression of Q^2/M_{QCD}^2 compared to OPE in the form of dimensional coefficients $\propto \rho^2, m_\pi^2, q^2$ divided by $(4\pi f_\pi)^2$. When the Roper is integrated out, these terms are replaced by analytic terms suppressed by powers of $\{q, m_\pi\}/\rho$ in addition to $\{q^2, m_\pi^2\}/(4\pi f_\pi)^2$. The one-Roper contributions proportional to $1/\rho$ take the form

$$V_C^{(1R)} = -\frac{3g_A^2 g_A'^2}{64\pi f_\pi^4 \rho} \left[m_\pi \omega^2(q) + (2m_\pi^2 + q^2)^2 A(q) \right], \quad (24)$$

$$W_C^{(1R)} = 0, \quad (25)$$

$$V_T^{(1R)} = -V_S^{(1R)} = 0, \quad (26)$$

$$W_T^{(1R)} = -W_S^{(1R)} = -\frac{g_A^2 g_A'^2 q^2}{64\pi f_\pi^4 \rho} [m_\pi + \omega^2(q) A(q)]. \quad (27)$$

Actually, the above equations for V_C and W_T/W_S are exact. As expected, this potential has the form of the subleading TPE with the substitution of $g_A'^2/(2\rho) \rightarrow c_4 = -2c_3$. The relation between c_3 and c_4 is the same as that shown in Ref. [67] for the Roper saturation, wherein $c_4^R = -2c_3^R = g_A^2 \bar{R}/(8\rho)$ with $\bar{R} = 0.28$. Notice a value of $g_A' \approx 0.34$ ($\rho = 470\text{MeV}$) is suggested by the Roper saturation by comparing the two relations of c_3 and c_4 . Such a value is consistent with the “N³LO EFT” value listed in Table I of Ref. [48]. Moreover, the values of g_A' and ρ used in this work (shown in the next section) suggest that $c_3^R \approx -0.41 \text{ GeV}^{-1}$ and $c_3^R \approx 0.82 \text{ GeV}^{-1}$. Their values are much larger than those shown in Ref. [67] ($c_3^R = -0.06 \text{ GeV}^{-1}$ and $c_4^R = 0.12 \text{ GeV}^{-1}$), implying an enhancement in the contribution to the potential from the intermediate Roper resonance at this order.

The form of the potential and its effects on observables are studied in the next section.

III. NUMERICAL RESULTS AND DISCUSSION

The Roper TPE potential is determined in terms of one-baryon LECs. After we discuss their values, we present plots of the potential and its effects on the phase shifts of high partial waves.

A. Values of LECs

To calculate the NN scattering phase shifts, we must fix all relevant LECs. The LO nucleon axial-vector coupling is fixed at $g_A = 1.29$, the pion decay constant at $f_\pi = 92.4$ MeV, the pion mass at $m_\pi = 139$ MeV, and the nucleon mass at $m_N = 939$ MeV. The exact values of these LECs are not very important, as the Roper parameters are much less well known and their uncertainties dominate the uncertainty of our results.

For illustration, for the nucleon-Roper coupling g'_A and mass splitting ρ , we adopt the values listed in Table I of Ref. [48], which are extracted from fits to πN data in HB χ PT with an explicit Roper where the nucleon parameters take the values listed above. We focus on the “N²LO EFT” values, that is $g'_A = 1.06$ and $\rho = 690$ MeV, which are obtained from a fit to the GW phase-shift analysis (PSA) [68] near the Delta resonance. In this region, Delta effects are enhanced by two orders, so in the Roper-nucleon sector “N²LO EFT” includes only the parameters we consider here. This set of LECs is therefore consistent from an EFT perspective. However, these values are quite far from those corresponding to a reducible representation of the chiral group [49, 50], which is suggested by the saturation of the Adler-Weisberger sum rule. Alternative numerical studies have also been performed here with the “N³LO EFT” and “N²LO GW” values of g'_A and ρ listed in Table I of Ref. [48], which are close to those from a chiral reducible representation. The first set of values ($g'_A = 0.32$ and $\rho = 470$ MeV) is obtained from a πN phase-shift fit that includes also a parameter of the subleading nucleon-Roper Lagrangian, $\mathcal{L}^{(1)}$. The second set of values ($g'_A = 0.54$ and $\rho = 550$ MeV) is fitted at the same order considered here, but to the values of the Breit-Wigner mass and width extracted from the GW PSA [68]. For both sets of values, the Roper effects are enhanced by the smaller mass splitting but reduced by the smaller couplings. The results here are *qualitatively* consistent with those obtained with the “N²LO EFT” LECs with an insignificant difference even at large laboratory energies.

As discussed in the previous section, the singularity of pion exchange means the separation

between long- and short-range effects is model dependent: in addition to the pion, one-nucleon and one-Roper LECs, the TPE potential depends on the renormalization scale μ . Since we expect the scale characterizing short-range effects to be $M_{\text{QCD}} \sim 1$ GeV, we take $\mu = 1$ GeV for illustration. This corresponds to a natural size of the associated NN LECs.

B. The potential as a function of momentum transfer

The potential is not observable, as its short-range part is regulator dependent to ensure that the full amplitude, from which observables are extracted, is properly renormalized. Nevertheless, the long-range part of the potential (given by the non-analytic terms) provides some intuition about its effects on the full amplitude. In Fig. 2 we compare, as a function of the momentum transfer q , the various components of the TPE potential from the Roper/one-Roper — denoted R/1R — to those from the leading TPE potential and the subleading TPE potential with the values of $c_{1,3,4}$ taken as explained — denoted TPE and Sat.

The largest components from the Roper are central. Without the Roper, The first contribution to the isoscalar central force V_C arises from the subleading TPE potential, which is one order higher than that considered here. The 2R contribution to V_C , Eq.(6), is strongly repulsive, but its strength is almost independent from the transferred momentum q , and consequently can be absorbed into the short-range part to a greater or lesser extent. The 1R and Sat. contributions to the V_C are attractive and identical. In contrast, the isovector central force W_C receives the first contribution at the same order in Roperless and Roperful EFTs. The contribution to W_C in both EFTs is repulsive, with different behaviors and strengths. In Roperful EFT, the 1R contribution to W_C arises from terms proportion to $\rho^{-2,0,2,\dots}$ and is almost independent of q . The 2R contribution thus dominates the Roper contribution to the phaseshifts for W_C . In TPE at this order, W_C increases with q at about the same rate as W_C in R. As shown in Eq. (25), there is no contribution to W_C from Sat. at this order.

The other components of the R potentials are smaller in magnitude, with spin-spin and quasi-tensor contributions differing only in sign. Because the football and triangle diagrams do not contribute to quasi-tensor and spin-spin forces, and $V_T = -V_S$ and $W_T = -W_S$ in box diagrams, the behaviors of the spin-spin and quasi-tensor potentials are similar in both EFTs. For the isoscalar components, there is a contribution at the same order in TPE which is nearly five times as strong as the R potential (Eqs. (9), (11) and (10), (12)). The isovector components in R (Eqs. (13), (15) and (14), (16)) are larger by a factor ~ 2 compared to the isoscalar components with different

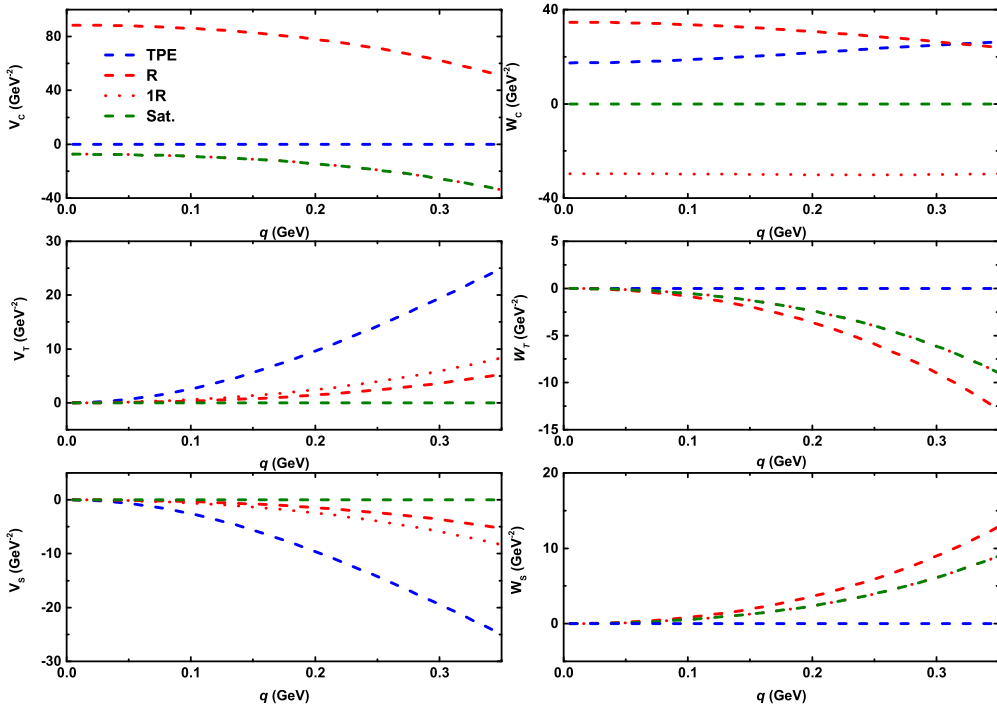


FIG. 2: Isoscalar (left panel) and isovector (right panel) components of the two-nucleon potential in units of GeV^{-2} , as a function of the transferred momentum q in GeV : central (top), tensor multiplied by q^2 (middle), and spin-spin (bottom). The blue (red) dashed lines denote the contributions from two-pion exchanges without (solely from) intermediate Roper contributions. The red dotted lines represent contributions from two-pion exchanges via a single intermediate Roper state. The Green dashed lines refer to the contributions from subleading two-pion exchanges with $c_1 = 0, c_3 = -\frac{1}{2}c_4 = -\frac{g_A'^2}{4\rho}$.

signs. There is no TPE contribution at the same order, but the isovector tensor component of R is minuscule compared to OPE. Again, the 1R contributions to W_T, W_S are identical to the Sat. contributions as shown in Eq.(27). The 2R contributions to the tensor and spin components are less than half of the 1R contributions.

C. Phase shifts and mixing angles of high partial waves

To quantify the effects of the Roper on observables, we calculate NN scattering of high partial waves. The short-range part of our potential, which cannot be separated from contact interactions in a model-independent way, contributes only to waves with orbital angular momentum $L \leq 1$. To focus on the long-range part of the potential, which can be attributed to the Roper, we consider

phase shifts with $L \geq 2$ and mixing angles with $J \geq 2$.

The NN scattering phase shifts and mixing angles can be obtained by using the “Stapp” — or “bar” — parameterization [69] of the S matrix, which is related to the on-shell T matrix. To obtain the on-shell T matrix, one must insert the potential into a scattering equation, such as the Lippmann-Schwinger equation. However, for large angular momenta, the centrifugal barrier effectively reduces the effects of the potential by inverse factors of L . The suppression is stronger for shorter-range components of the potential, as the centrifugal barrier more effectively shields them. As a consequence, partial waves with $L \geq 2$ probe predominantly the long-range components of the potential, which can be treated perturbatively [70–75]. For these waves, phase shifts are essentially monotonic and relatively small, $|\delta| \lesssim 30^\circ$, in which case $\tan \delta \approx \delta$. The difference between phase shifts obtained in the scattering equation and in perturbation theory is then small. The Roper effects can be seen in the phase shifts and mixing angles calculated in first-order perturbation theory,

$$\delta_{LSJ} = -\frac{m_N^2 p}{4\pi E} \operatorname{Re} \langle LSJ | V | LSJ \rangle, \quad (28)$$

$$\varepsilon_J = -\frac{m_N^2 p}{4\pi E} \operatorname{Re} \langle J-1, 1, J | V | J+1, 1, J \rangle. \quad (29)$$

where p and $E = \sqrt{m_N^2 + p^2}$ are the CM momentum and energy, respectively, and $|LSJ\rangle$ is the free wavefunction in the basis of well-defined orbital angular momentum, spin, and total angular momentum. On-shell, the transferred momentum $q = |\vec{q}| = p\sqrt{2(1-z)}$, $z = \cos \theta$, with θ the scattering angle. The exclusion principle constrains the isospin I so that $I + S + L$ is odd. The matrix elements can be written as angular integrals of the isospin-projected combinations

$$U_K = V_K + (4I - 3)W_K, \quad K = C, S, T, \quad (30)$$

multiplied by Legendre polynomials of degree J or $J \pm 1$, $P_J(z)$ or $P_{J\pm 1}(z)$. The explicit partial-wave projections can be found in Ref. [10]. Note that the kinematical prefactors differ from those of Ref. [10] due to a different sign convention for the potential V . Using a more consistent energy $E = m_N$ yields less than 7% discrepancies in phase shifts at laboratory energies T_{lab} near the pion-production threshold.

D -, F -, and G -wave phase shifts as well as the mixing angles $\epsilon_{2,3,4}$ are shown in Figs. 3 to 5 as a function of the laboratory energy $T_{\text{lab}} = 2p^2/m_N$ up to near the pion-production threshold (≈ 280 MeV). Results are shown for OPE [10] and for successive additions to OPE: formally leading TPE

without Roper [10], including Roper (Eqs. (5) to (16)), including only one-intermediate Roper, and including subleading TPE with $c_{1,3,4}$. For both For the F (Fig. 4) and G (Fig. 5) waves, the phase is on the order of a few degrees. Contributions from TPE are small compared to those of LO OPE, with Roper contributions barely visible on the scale of the figures. The shorter-range effects of TPE, particularly the Roper part, are increasingly suppressed in higher waves. For example, OPE dominates over Roperless leading and subleading TPE in H and I waves [10, 11]. In contrast, the D -wave phase shifts (Fig. 3) tend to be larger, indicating the increasing effects of the interactions. As expected, the relative effects of the TPE potentials are largest in D waves.

The contributions from the intermediate Roper are sizeable and account for nearly one half of the conventional TPE, except 3D_1 , where it is very small, and 3D_3 where it is even larger than the conventional TPE. For all partial waves, the Roper TPE effects are smaller than those of purely nucleonic TPE at the same order. Because of the effectively shorter range of the Roper TPE due to the Roper mass, relative Roper effects tend to increase with energy.

The NN scattering phase shifts for $L \geq 2$ and mixing angles for $J \geq 2$ receive no contribution from the analytic terms in the potential (Eqs. (5) to (16)) or the associated LECs. Results can be explained by referring to the components of the isoscalar and isovector TPE potential shown in Fig. 2, together with the projection with Legendre polynomials. For $I = 0$, the central combinations with and without Roper, $U_C(R)$ and $U_C(\mathcal{R})$, are both attractive. While $U_C(\mathcal{R})$ decreases with q , $U_C(R)$ increases gently for $q \lesssim 0.25$ GeV because of a cancellation between $V_C(R)$ and $W_C(R)$. For $I = 1$, this behavior is changed, i.e., $U_C(R)$ retains the features of $V_C(R)$ and $W_C(R)$, with its strength being approximately 100 GeV $^{-2}$ larger than that of $U_C(\mathcal{R})$ for the q region plotted here. Nevertheless, the contributions to the matrix elements from $U_C(R)$ and $U_C(\mathcal{R})$ in high partial waves are of similar magnitude because U_C is always multiplied with a Legendre polynomial, and the contribution from a constant term vanishes after the angular integration. Therefore, for $I = 1$, if one shifts $U_C(R)$ downwards by about 100 GeV $^{-2}$, $U_C(R)$ decreases with the momentum at about 6 times rate as $U_C(\mathcal{R})$ increases with q . Their contributions to the matrix elements differ in relatively low waves, e.g., the D Wave, and this difference is suppressed for higher waves due to the higher-order Legendre polynomials. For spin S , spin-spin and central terms enter the combination $U_C + (4S - 3)U_S$. While the spin factor is insufficient to compensate for the larger magnitude of $U_C(R)$ for $I = 1$ channels, the spin-spin and central terms are comparable for $I = 0$. The quasi-tensor force contributes to matrix elements separately and is responsible for non-zero mixing angles with our potential. Like for the spin-spin component, the contributions from the quasi-tensor force in $U(R)$ and $U(\mathcal{R})$ are of the same magnitude for both $I = 0$ and $I = 1$.

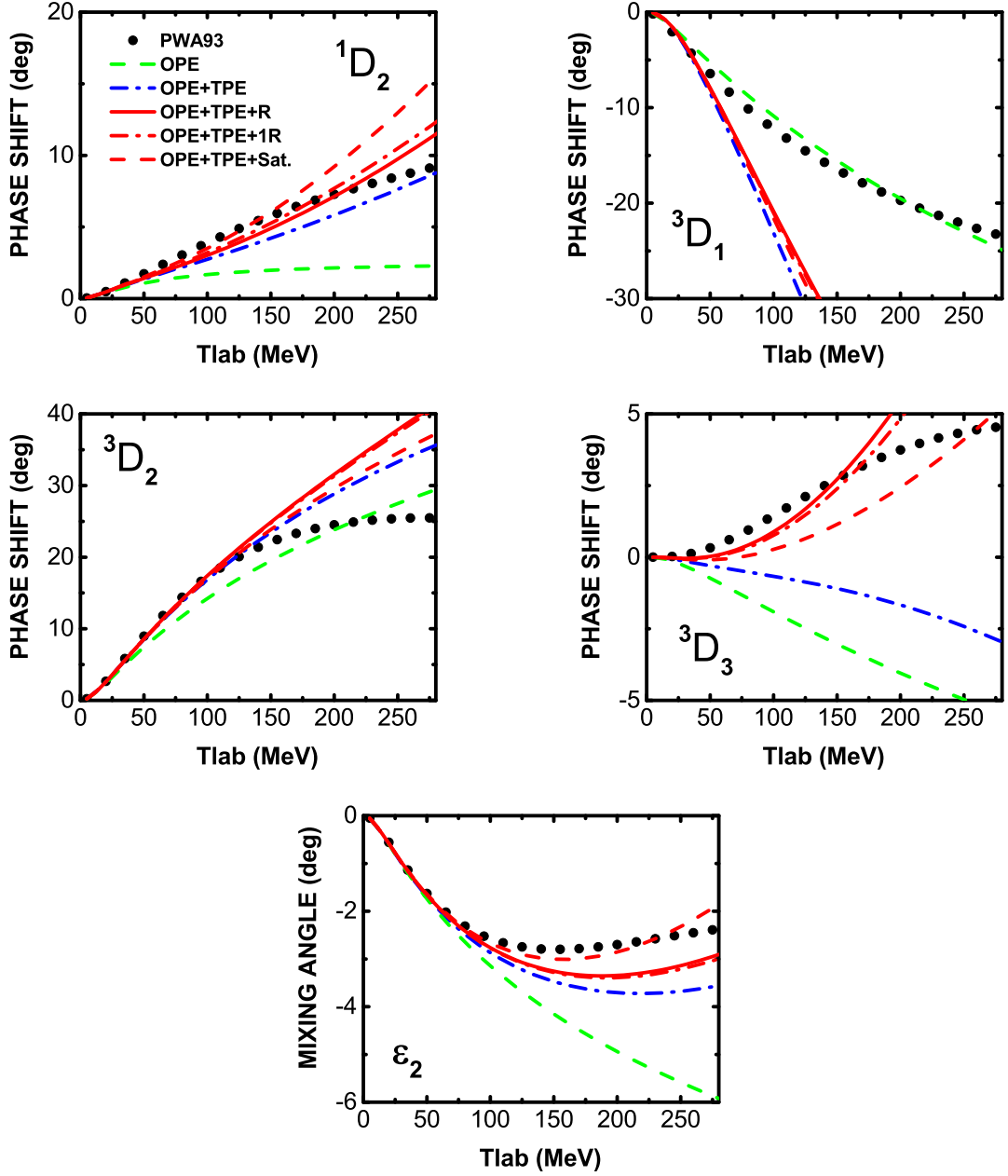


FIG. 3: D -wave phase shifts $^{2S+1}D_J$ and mixing angle ε_2 (in degrees) as a function of the laboratory energy T_{lab} (in units of MeV). The (green) dashed curves correspond to the OPE contributions, the (blue) dash-dotted curves represent the TPE contributions, and the (red) solid/dash-dotted/dashed curves represent the sum of OPE and TPE contributions, including those from the intermediate Roper resonance/intermediate one-Roper resonance/ subleading TPE with $c_{1,3,4}$ determined as explained in the text.

The (black) dots refer to the Nijmegen partial-wave phase shifts [76].

For $S = 0$, the potential enters in the combination $U_C - 3U_S - U_T$. The isospin $I = 1$ ($I = 0$) for L even (odd), for example 1D_2 and 1G_4 (1F_3). For the 1D_2 partial wave, contributions from central and quasi-tensor forces are comparable, with a different sign for both EFTs; the spin-spin

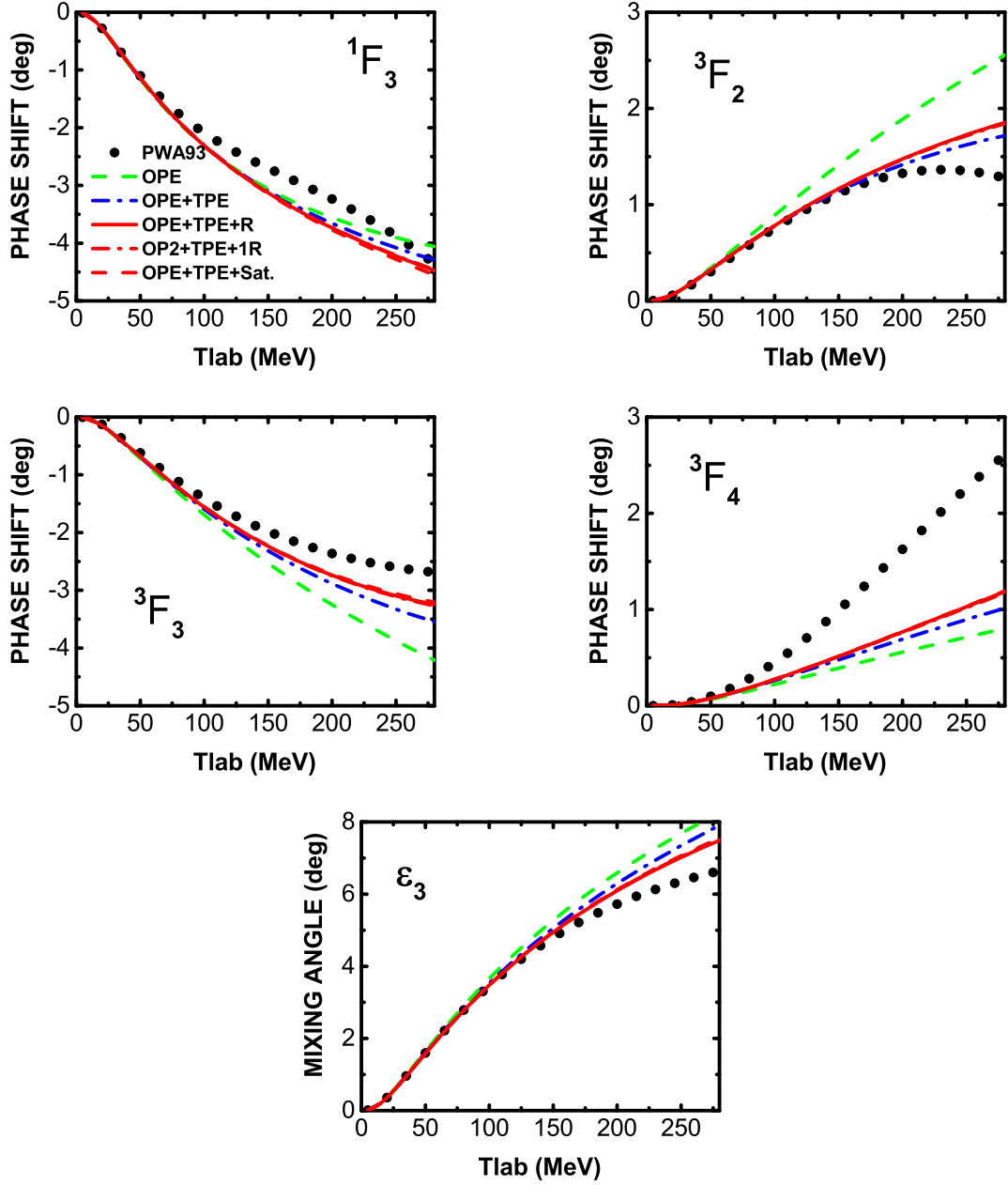


FIG. 4: Same as Fig. 3, but for the F -wave phase shifts $^{2S+1}F_J$ and mixing angle ε_3 .

force nearly saturates this channel. The Roper effects are very small for the 1F_3 and 1G_4 partial waves.

For $S = 1$, central and spin-spin potentials enter in the combination $U_C + U_S$, while U_T contributes with various angle combinations depending on whether $L = J$ or $L = J \pm 1$. Here, $I = 0$ ($I = 1$) for L even (odd), for example $^3D_{1,2,3}$, $^3G_{3,4,5}$ and ε_3 ($^3F_{2,3,4}$, $\varepsilon_{2,4}$). For all D waves, the phase shifts rise, and the description of data ameliorates with the inclusion of Roper, except for the 3D_2 partial wave. Among all the D waves, the Roper effects are the most significant for the

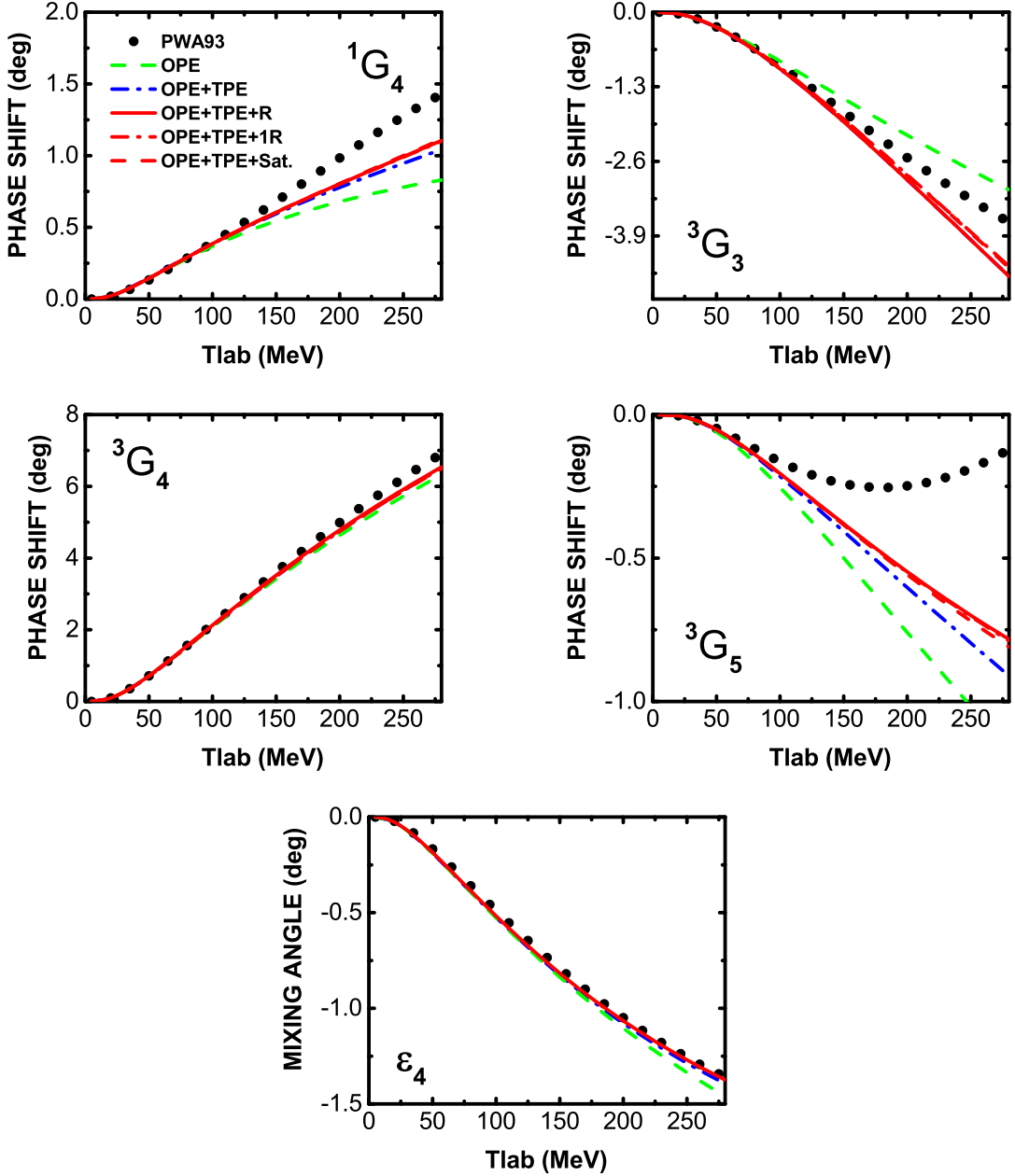


FIG. 5: Same as Fig. 3, but for the G -wave phase shifts $^{2S+1}G_J$ and mixing angle ε_4 .

3D_3 partial wave. For the 3D_3 partial wave, $S = 1$ and $I = 0$, the contribution from the tensor components ($U_T(R)$) get suppressed because of the pre-factor $\frac{2}{2J+1}$, the spin-spin ($U_S(R)$) and central ($U_C(R)$) forces are comparable and are responsible for the improvement of phase shifts. As seen in the D wave, including Roper quantitatively improved the description of phase shifts for F and G waves, although the Roper effects are small for these partial waves. The quasi-tensor force contributes to the mixing angles, which connect $L = J \pm 1$. The only sizable effect is in ε_2 , where the Roper effects shift the curves upwards like those seen in all D waves.

Our perturbative calculations of 3D_1 , ε_2 , and 3F_2 should be taken with a grain of salt. The tensor force connects 3D_1 to 3S_1 , where nonperturbative effects are sufficiently strong to produce the deuteron bound state. All present indications are that OPE needs to be treated nonperturbatively in these partial waves [70, 71, 73, 74, 77]. The tensor force also connects ε_2 and 3F_2 to 3P_2 , although perturbation theory might still work for these waves [75]. Although the Roper effects are seen to be relatively small, the inclusion of the Roper resonance in TPE leads to a better description of the results from the Nijmegen PSA [76], shown in Figs. 3 to 5 to illustrate what experimental data imply. For most channels, the descriptions are reasonably good, with the exception of 3D_1 , 3F_4 and 3G_5 — in those partial waves, our potential is too repulsive. As in any EFT, the description of data tends to deteriorate with energy, with higher-order contributions becoming relatively larger. Among those are the TPE potentials involving the Δ isobar. Without the Roper, Deltaful TPE [3, 7, 10] is relatively large and goes in the correct direction for these channels, except for 3D_1 — likely a limitation of perturbation theory.

IV. SUMMARY AND OUTLOOK

We calculated the leading NN two-pion-exchange potential with intermediate nucleon and Roper resonance in the HB χ PT. Analytic terms cannot be distinguished from low-energy constants that do not contribute to partial waves with $L \geq 2$. We found that for the isospin singlet, central, spin-spin, and tensor forces are comparable to formally leading TPE without baryon excitations. For the isospin triplet, the central force with the intermediate Roper resonance is significantly larger than that from TPE without it. Nevertheless, the huge difference is suppressed when projected to the LSJ basis. For the tensor and spin-spin forces, the potentials with Roper are approximately half/twice those without it for $I = 1/0$. With this potential, we obtained the phase shifts for D , F , and G waves in first-order perturbation theory and the mixing angles for $J = 2, 3, 4$. We found that the description of phase shifts and mixing angles is improved for all partial waves by including the intermediate Roper resonance. Moreover, the contributions from the Roper are found to be sizeable for D waves. Although the obtained phase shifts are in reasonable agreement with empirical results, there are still visible discrepancies for the 3D_1 , 3D_2 , 3F_4 , and 3G_5 partial waves. TPE mitigates some of these discrepancies in an EFT with nucleon and an explicit Delta isobar. It has long been noted that the subleading TPE potential in the absence of explicit baryon resonances is comparable or even larger than the formally leading TPE, mostly because of contributions to the low-energy constants c_3 and c_4 . Because of its relatively low mass, the Delta isobar is expected to be crucial in

the NN interaction [3, 7]. Indeed, the values of c_3 and c_4 are dominated by Δ saturation [67], and previous studies [11, 34] have shown that the leading TPE with the intermediate Delta is to some extent equivalent to the formally subleading TPE without Deltas. Contrary to the Δ saturation, the contribution to the values of the two LECs from the Roper saturation is minor [67]. From this point of view, the Roper resonance is not as important as the Delta isobar in NN scattering, as one might have expected from its larger mass. We compared TPE with an explicit Roper to subleading TPE with Roper-saturated c_3 and c_4 , which includes only the physics of one-Roper diagrams. We found a significant enhancement of the values of c_3 and c_4 from contributions of one-Roper diagrams compared to the values from the Roper resonance shown in Ref. [67], the enhanced values are still less than those from the Δ saturation and reduce to those in Ref. [67] when using the N³LO EFT values of g'_A and ρ in Ref. [48] in the calculation. Of course, in an EFT that includes the Roper explicitly, one must include an explicit Delta. Since the latter's effects are large in TPE, the combined Delta-Roper contributions could be non-negligible. Yet it is not accounted for in the formally subleading TPE without baryon resonances. We plan to address TPE from combined Delta-Roper resonances in a future publication.

Acknowledgments

This work is partly supported by the National Natural Science Foundation of China under Grant No.12435007, No.12505096, and the Chinese Postdoctoral Science Foundation under Grants No.2022M720360. This material is based upon work supported in part by the U.S. Department of Energy, Office of Science, Office of Nuclear Physics, under award DE-FG02-04ER41338.

Appendix A: Explicit expressions for TPE potentials with intermediate Roper resonance.

The explicit expressions of the TPE potentials for the Feynman diagrams shown in Fig. 1 are,

- Roper resonance in triangle diagrams:

$$W_C^{(1R\Delta)} = \frac{g_A^2 g_A'^2}{192\pi^2 f_\pi^4} \left[-2m_\pi^2 - \frac{13}{6}q^2 + 18\rho^2 - 19h\rho \cosh^{-1} \frac{\rho}{m_\pi} + (18m_\pi^2 + 5q^2 - 36\rho^2) \ln \frac{m_\pi}{\mu} \right. \\ \left. + (8m_\pi^2 + 5q^2 - 12\rho^2)L(q) - (6q^2 + 12h^2)f_1(q) \right]. \quad (\text{A1})$$

- Single Roper resonance in planar-box diagrams:

$$V_C^{(1R\square)} = -\frac{3}{2}W_C^{(1R\square)} \quad (A2)$$

$$= -\frac{g_A^2 g_A'^2}{256\pi^2 f_\pi^4} \left[32m_\pi^2 + \frac{67}{6}q^2 - 30\rho^2 + 6\pi \frac{m_\pi}{\rho} \omega^2(q) + (48\rho^2 - 12\omega^2(q)) \frac{h}{\rho} \cosh^{-1} \frac{\rho}{m_\pi} \right. \\ \left. - (90m_\pi^2 + 23q^2 - 60\rho^2) \ln \frac{m_\pi}{\mu} - (20m_\pi^2 + 11q^2 - 12\rho^2) L(q) \right. \\ \left. + 6\pi \frac{(2m_\pi^2 + q^2)^2}{\rho} A(q) + 3 \frac{(q^2 - 2h^2)^2}{\rho^2} f_1(q) \right], \quad (A3)$$

$$V_T^{(1R\square)} = -\frac{3}{2}W_T^{(1R\square)} = -V_S^{(1R\square)} = \frac{3}{2}W_S^{(1R\square)} \quad (A4)$$

$$= \frac{3g_A^2 g_A'^2 q^2}{128\pi^2 f_\pi^4} \left[2 + \frac{\pi m_\pi}{2\rho} - \frac{h}{\rho} \cosh^{-1} \frac{\rho}{m_\pi} - 2 \ln \frac{m_\pi}{\mu} - L(q) + \pi \frac{\omega^2(q)}{2\rho} A(q) - \left(1 - \frac{\omega^2(q)}{4\rho^2} \right) f_1(q) \right]. \quad (A5)$$

- Single Roper resonance in crossed-box diagrams:

$$V_C^{(1R\boxtimes)} = \frac{3}{2}W_C^{(1R\boxtimes)} \quad (A6)$$

$$= -\frac{g_A^2 g_A'^2}{256\pi^2 f_\pi^4} \left[-32m_\pi^2 - \frac{67}{6}q^2 + 30\rho^2 + 6\pi \frac{m_\pi}{\rho} \omega^2(q) - (48\rho^2 - 12\omega^2(q)) \frac{h}{\rho} \cosh^{-1} \frac{\rho}{m_\pi} \right. \\ \left. + (90m_\pi^2 + 23q^2 - 60\rho^2) \ln \frac{m_\pi}{\mu} + (20m_\pi^2 + 11q^2 - 12\rho^2) L(q) \right. \\ \left. + 6\pi \frac{(2m_\pi^2 + q^2)^2}{\rho} A(q) - 3 \frac{(q^2 - 2h^2)^2}{\rho^2} f_1(q) \right], \quad (A7)$$

$$V_T^{(1R\boxtimes)} = \frac{3}{2}W_T^{(1R\boxtimes)} = -V_S^{(1R\boxtimes)} = -\frac{3}{2}W_S^{(1R\boxtimes)} \quad (A8)$$

$$= \frac{3g_A^2 g_A'^2 q^2}{128\pi^2 f_\pi^4} \left[2 - \frac{\pi m_\pi}{2\rho} - \frac{h}{\rho} \cosh^{-1} \frac{\rho}{m_\pi} - 2 \ln \frac{m_\pi}{\mu} - L(q) - \pi \frac{\omega^2(q)}{2\rho} A(q) - \left(1 - \frac{\omega^2(q)}{4\rho^2} \right) f_1(q) \right]. \quad (A9)$$

- Double Roper resonance in planar-box diagrams:

$$V_C^{(2R\square)} = -\frac{3}{2}W_C^{(2R\square)} \quad (A10)$$

$$= \frac{g_A'^4}{512\pi^2 f_\pi^4} \left[-32m_\pi^2 - \frac{67}{6}q^2 + 30\rho^2 + (12\omega^2(q) - 48\rho^2) \frac{h}{\rho} \cosh^{-1} \frac{\rho}{m_\pi} \right. \\ \left. + (90m_\pi^2 + 23q^2 - 60\rho^2) \ln \frac{m_\pi}{\mu} + (20m_\pi^2 + 11q^2 - 12\rho^2) L(q) - 3 \frac{(q^2 - 2h^2)^2}{\rho^2} f_1(q) \right], \quad (A11)$$

$$V_T^{(2R\square)} = -\frac{3}{2}W_T^{(2R\square)} = -V_S^{(2R\square)} = \frac{3}{2}W_S^{(2R\square)} \quad (A12)$$

$$= \frac{3g_A'^4 q^2}{256\pi^2 f_\pi^4} \left[2 - \frac{h}{\rho} \cosh^{-1} \frac{\rho}{m_\pi} - 2 \ln \frac{m_\pi}{\mu} - L(q) - \left(1 - \frac{\omega^2(q)}{4\rho^2} \right) f_1(q) \right]. \quad (A13)$$

- Double Roper resonance in crossed-box diagrams:

$$V_C^{(2R\boxtimes)} = \frac{3}{2}W_C^{(2R\boxtimes)} \quad (A14)$$

$$= - \frac{g_A'^4}{512\pi^2 f_\pi^4} \left[16m_\pi^2 + \frac{5}{6}q^2 + 42\rho^2 + (12q^2 - 144h^2) \frac{\rho}{h} \cosh^{-1} \frac{\rho}{m_\pi} \right. \\ \left. + (90m_\pi^2 + 23q^2 - 180\rho^2) \ln \frac{m_\pi}{\mu} + (20m_\pi^2 + 11q^2 - 36\rho^2) L(q) \right. \\ \left. + 24(q^2 - 2h^2) f_1(q) - 3 \frac{(q^2 - 2h^2)^2}{\rho^2} f_2(q) \right], \quad (A15)$$

$$V_T^{(2R\boxtimes)} = \frac{3}{2}W_T^{(2R\boxtimes)} = -V_S^{(2R\boxtimes)} = -\frac{3}{2}W_S^{(2R\boxtimes)} \quad (A16)$$

$$= \frac{3g_A'^4 q^2}{256\pi^2 f_\pi^4} \left[1 - \frac{\rho}{h} \cosh^{-1} \frac{\rho}{m_\pi} - 2 \ln \frac{m_\pi}{\mu} - L(q) - 2f_1(q) - \left(1 - \frac{\omega^2(q)}{4\rho^2} \right) f_2(q) \right]. \quad (A17)$$

[1] S. Weinberg, Phys. Lett. B **251**, 288 (1990).

[2] S. Weinberg, Nucl. Phys. B **363**, 3 (1991).

[3] C. Ordóñez and U. van Kolck, Phys. Lett. B **291**, 459 (1992).

[4] S. Weinberg, Phys. Lett. B **295**, 114 (1992), hep-ph/9209257.

[5] C. Ordóñez, L. Ray, and U. van Kolck, Phys. Rev. Lett. **72**, 1982 (1994).

[6] U. van Kolck, Phys. Rev. C **49**, 2932 (1994).

[7] C. Ordóñez, L. Ray, and U. van Kolck, Phys. Rev. C **53**, 2086 (1996), hep-ph/9511380.

[8] H.-W. Hammer, S. König, and U. van Kolck, Rev. Mod. Phys. **92**, 025004 (2020), 1906.12122.

[9] S. Weinberg, Physica A **96**, 327 (1979).

[10] N. Kaiser, R. Brockmann, and W. Weise, Nucl. Phys. A **625**, 758 (1997), nucl-th/9706045.

- [11] N. Kaiser, S. Gerstendörfer, and W. Weise, Nucl. Phys. A **637**, 395 (1998), nucl-th/9802071.
- [12] E. E. Jenkins and A. V. Manohar, Phys. Lett. B **255**, 558 (1991).
- [13] E. E. Jenkins and A. V. Manohar, Phys. Lett. B **259**, 353 (1991).
- [14] R. Machleidt and D. R. Entem, Phys. Rept. **503**, 1 (2011), 1105.2919.
- [15] E. Epelbaum, H. Krebs, and P. Reinert, Front. in Phys. **8**, 98 (2020), 1911.11875.
- [16] X.-L. Ren, K.-W. Li, L.-S. Geng, B.-W. Long, P. Ring, and J. Meng, Chin. Phys. C **42**, 014103 (2018), 1611.08475.
- [17] Y. Xiao, L.-S. Geng, and X.-L. Ren, Phys. Rev. C **99**, 024004 (2019), 1812.03005.
- [18] Y. Xiao, C.-X. Wang, J.-X. Lu, and L.-S. Geng, Phys. Rev. C **102**, 054001 (2020), 2007.13675.
- [19] Q.-Q. Bai, C.-X. Wang, Y. Xiao, and L.-S. Geng, Phys. Lett. B, 135745 (2020), 2007.01638.
- [20] C.-X. Wang, L.-S. Geng, and B. Long, Chin. Phys. C **45**, 054101 (2021), 2001.08483.
- [21] X.-L. Ren, C.-X. Wang, K.-W. Li, L.-S. Geng, and J. Meng, Chin. Phys. Lett. **38**, 062101 (2021), 1712.10083.
- [22] C.-X. Wang, J.-X. Lu, Y. Xiao, and L.-S. Geng (2021), 2110.05278.
- [23] Q.-Q. Bai, C.-X. Wang, Y. Xiao, and L.-S. Geng (2021), 2105.06113.
- [24] J.-X. Lu, C.-X. Wang, Y. Xiao, L.-S. Geng, J. Meng, and P. Ring (2021), 2111.07766.
- [25] Y. Xiao, J.-X. Lu, and L.-S. Geng, Phys. Rev. C **110**, 064002 (2024), 2406.01292.
- [26] J.-X. Lu, Y. Xiao, Z.-W. Liu, and L.-S. Geng, Int. J. Mod. Phys. E **34**, 2543007 (2025), 2501.17185.
- [27] Y. Xiao, J.-X. Lu, and L.-S. Geng (2025), 2504.15598.
- [28] J.-X. Lu and L.-S. Geng (2025), 2511.18023.
- [29] D. R. Entem, R. Machleidt, and Y. Nosyk, Phys. Rev. C **96**, 024004 (2017), 1703.05454.
- [30] M. Pavón Valderrama, AIP Conf. Proc. **1322**, 205 (2010), 1009.6100.
- [31] M. Pavón Valderrama (2019), 1902.08172.
- [32] C. Mishra, A. Ekström, G. Hagen, T. Papenbrock, and L. Platter (2021), 2111.15515.
- [33] M. Pavón Valderrama (2021), 2112.02076.
- [34] H. Krebs, E. Epelbaum, and U.-G. Meißner, Eur. Phys. J. A **32**, 127 (2007), nucl-th/0703087.
- [35] E. Epelbaum, H. Krebs, and U.-G. Meißner, Phys. Rev. C **77**, 034006 (2008), 0801.1299.
- [36] M. Piarulli, L. Girlanda, R. Schiavilla, R. Navarro Pérez, J. E. Amaro, and E. Ruiz Arriola, Phys. Rev. C **91**, 024003 (2015), 1412.6446.
- [37] A. Ekström, G. Hagen, T. D. Morris, T. Papenbrock, and P. D. Schwartz, Phys. Rev. C **97**, 024332 (2018), 1707.09028.
- [38] S. Strohmeier and N. Kaiser, Nucl. Phys. A **1002**, 121980 (2020), 2004.12964.
- [39] Y. Nosyk, D. R. Entem, and R. Machleidt, Phys. Rev. C **104**, 054001 (2021), 2107.06452.
- [40] V. R. Pandharipande, D. R. Phillips, and U. van Kolck, Phys. Rev. C **71**, 064002 (2005), nucl-th/0501061.
- [41] E. Epelbaum, H. Krebs, and U.-G. Meißner, Nucl. Phys. A **806**, 65 (2008), 0712.1969.
- [42] N. Kaiser, Phys. Rev. C **92**, 024002 (2015), 1504.05131.

- [43] H. Krebs, A. M. Gasparyan, and E. Epelbaum, Phys. Rev. C **98**, 014003 (2018), 1803.09613.
- [44] D. Logoteta, I. Bombaci, and A. Kievsky, Phys. Rev. C **94**, 064001 (2016), 1609.00649.
- [45] B. Long and U. van Kolck, Nucl. Phys. A **840**, 39 (2010), 0907.4569.
- [46] V. Pascalutsa and D. R. Phillips, Phys. Rev. C **67**, 055202 (2003), nucl-th/0212024.
- [47] L. D. Roper, Phys. Rev. Lett. **12**, 340 (1964).
- [48] B. Long and U. van Kolck, Nucl. Phys. A **870-871**, 72 (2011), 1105.2764.
- [49] S. Weinberg, Phys. Rev. **177**, 2604 (1969).
- [50] S. R. Beane and U. van Kolck, J. Phys. G **31**, 921 (2005), nucl-th/0212039.
- [51] B. Borasoy, P. C. Bruns, U.-G. Meißner, and R. Lewis, Phys. Lett. B **641**, 294 (2006), hep-lat/0608001.
- [52] D. Djukanovic, J. Gegelia, and S. Scherer, Phys. Lett. B **690**, 123 (2010), 0903.0736.
- [53] T. Bauer, S. Scherer, and L. Tiator, Phys. Rev. C **90**, 015201 (2014), 1402.0741.
- [54] J. Gegelia, U.-G. Meißner, and D.-L. Yao, Phys. Lett. B **760**, 736 (2016), 1606.04873.
- [55] M. Gelenava, Eur. Phys. J. A **54**, 88 (2018), 1711.03494.
- [56] D. Severt and U.-G. Meißner, Commun. Theor. Phys. **72**, 075201 (2020), 2003.05745.
- [57] E. L. Lomon, Phys. Rev. D **26**, 576 (1982).
- [58] T.-S. H. Lee, Phys. Rev. C **29**, 195 (1984).
- [59] L. Ray, Phys. Rev. C **35**, 1072 (1987).
- [60] W. P. Sitarski, P. G. Blunden, and E. L. Lomon, Phys. Rev. C **36**, 2479 (1987).
- [61] S. Weinberg, Phys. Rev. **166**, 1568 (1968).
- [62] S. R. Coleman, J. Wess, and B. Zumino, Phys. Rev. **177**, 2239 (1969).
- [63] C. G. Callan, Jr., S. R. Coleman, J. Wess, and B. Zumino, Phys. Rev. **177**, 2247 (1969).
- [64] A. Manohar and H. Georgi, Nucl. Phys. B **234**, 189 (1984).
- [65] U. van Kolck, Eur. Phys. J. A **56**, 97 (2020), 2003.09974.
- [66] J. L. Friar, Phys. Rev. C **60**, 034002 (1999), nucl-th/9901082.
- [67] V. Bernard, N. Kaiser, and U.-G. Meißner, Nucl. Phys. A **615**, 483 (1997), hep-ph/9611253.
- [68] R. A. Arndt, W. J. Briscoe, I. I. Strakovsky, and R. L. Workman, Phys. Rev. C **74**, 045205 (2006), nucl-th/0605082.
- [69] H. P. Stapp, T. J. Ypsilantis, and N. Metropolis, Phys. Rev. **105**, 302 (1957).
- [70] A. Nogga, R. G. E. Timmermans, and U. van Kolck, Phys. Rev. C **72**, 054006 (2005), nucl-th/0506005.
- [71] M. C. Birse, Phys. Rev. C **74**, 014003 (2006), nucl-th/0507077.
- [72] M. Pavón Valderrama, M. Sánchez Sánchez, C. J. Yang, B. Long, J. Carbonell, and U. van Kolck, Phys. Rev. C **95**, 054001 (2017), 1611.10175.
- [73] S. Wu and B. Long, Phys. Rev. C **99**, 024003 (2019), 1807.04407.
- [74] D. B. Kaplan, Phys. Rev. C **102**, 034004 (2020), 1905.07485.
- [75] R. Peng, S. Lyu, and B. Long, Commun. Theor. Phys. **72**, 095301 (2020), 2011.13186.
- [76] V. G. J. Stoks, R. A. M. Klomp, M. C. M. Rentmeester, and J. J. de Swart, Phys. Rev. C **48**, 792 (1993).

[77] S. Fleming, T. Mehen, and I. W. Stewart, Nucl. Phys. A **677**, 313 (2000), nucl-th/9911001.